Aging and Disease
www.aginganddisease.org
Early access date: October 9, 2025
http://dx.doi.org/10.14336/AD.2025.0760

Original Article

Enhancing Mitochondrial Matrix Antioxidant SOD2 in Astrocytes Mitigates Cellular Senescence and Cognitive Impairment in Aging

Matthew P Baier[1,2], Sophia I Sharum[1], Jenna L Wilson[1], Sanjit Narasimhan[1], Chinnu Salim[1], Sreemathi Logan[1,2*]

[1]Department of Biochemistry and Physiology, The University of Oklahoma Health Campus, Oklahoma City, OK, USA. [2]Center for Geroscience and Healthy Brain Aging, The University of Oklahoma Health Campus, Oklahoma City, OK, USA.

[Received June 16, 2025; Revised September 26, 2025; Accepted October 4, 2025]

ABSTRACT: Accumulating evidence implicates hallmarks of brain aging, namely oxidative stress, reactive gliosis, and cellular senescence, as key contributors to hippocampal dysfunction and associated age-related cognitive deficits. Astrocytes robustly express antioxidants such as superoxide dismutases to detoxify reactive oxygen species (ROS) generated as a result of the high metabolic activity in the brain. However, aging is associated with transcriptional downregulation of antioxidant genes concomitant with polarization towards reactive, proinflammatory phenotypes in astrocytes. Given prior findings that astrocyte-specific ablation of SOD2 induces phenotypes of cognitive aging, we hypothesized that enhancing astrocyte antioxidant capacity via SOD2 overexpression (aSOD2OE) would ameliorate molecular hallmarks of aging and preserve cognitive function. To test this, we overexpressed SOD2 in astrocytes of aged (22 mo) male C57Bl/6N mice using an AAV(PHP.eB)-GFAP-hSOD2 viral vector and assessed hippocampal-dependent spatial working memory using a high-resolution, automated home-cage behavioral testing platform. We found that aSOD2OE significantly improved spatial working memory performance compared to aged GFP controls. Using molecular and histological approaches, aSOD2OE was associated with reductions in markers of cellular senescence and reactive astrogliosis within the hippocampus. These findings suggest that enhancement of astrocyte mitochondrial antioxidant activity is sufficient to alleviate maladaptive cellular programs associated with cognitive decline. Together, these data identify astrocyte redox biology as a potential therapeutic target in preserving hippocampal function in aging.

Keywords: aging, cognition, learning and memory, SOD2, reactive astrogliosis, cellular senescence

INTRODUCTION

Aging is the greatest risk factor for the development of chronic disease, including cognitive impairment and Alzheimer's disease related dementias (ADRD), that is marred with metabolic and structural deficits in the brain. Among factors though to contribute to age-related declines in hippocampal-dependent memory and learning are hallmarks of aging, including oxidative stress, inflammation, and cellular senescence [1]. The brain has a high metabolic demand, consuming 20% of the body's energy intake despite constituting of only 2% of the total body mass. This high energy demand required for neural activity is supported by astrocytes that regulate brain redox homeostasis [2, 3] through robust expression of glutathione and superoxide dismutases (SOD) [3], among others, that detoxify reactive oxygen species (ROS). Notably, hippocampal astrocytes show downregulation of multiple antioxidant genes in reactive astrocytes with age [4], and under some pathological conditions, astrocytes become a major source of detrimental ROS [5].

***Correspondence should be addressed to:** Dr. Sreemathi Logan, Department of Biochemistry and Physiology, The University of Oklahoma Health Campus, Oklahoma City, OK, USA. Email: Sreemathi-Logan@ou.edu.

Manganese superoxide dismutase (SOD2) is the primary mitochondrial antioxidant that quenches superoxide to hydrogen peroxide. Levels of superoxide have been shown to increase in the brain with age across multiple vertebrate species [6], and is associated with decreased transcriptional levels of *Sod2* in the hippocampus of aged mice [7]. Our lab and others have shown that astrocyte-specific SOD2 knockout (aSOD2KO) in middle- and late-aged mice resulted in phenotypes of cognitive aging, including spatial working memory deficits and increased reactive astrogliosis [7, 8]. These data suggest that the integrity of astrocyte antioxidant capacity is critical in maintaining cognitive health during the aging process.

Increased ROS and damage to macromolecules, including DNA, protein, and lipids [9] are interrelated hallmarks of aging linked to cellular senescence [1]. Senescent cells, characterized by cell cycle arrest and secretion of proinflammatory factors deemed the senescence-associated secretory phenotype (SASP), have been implicated in the pathogenesis of AD-like disease in various models, as well as in models of age-related cognitive decline [10-13]. We have previously shown that using cognitive stratification of aged animals, cognitively impaired mice are delineated from intact mice by increased hippocampal oxidative damage, reactive astrogliosis and cellular senescence [13, 14]. Importantly, deficiency of SOD2 is sufficient to drive DNA damage and induction of cellular senescence and aging phenotypes in the brain [8] and other tissues [15].

Taken together, these data suggest that cognitive deficits with age may be mediated in part by the decline in astrocyte antioxidant capacity that drives accumulation of senescent cells and increased reactive astrogliosis within the brain. Therefore, we hypothesized that astrocyte-specific overexpression of SOD2 (aSOD2OE) will protect against spatial working memory deficits by reducing senescence and reactive gliosis burden in the aged brain. Here, we report that enhancing astrocyte mitochondrial antioxidant capacity via aSOD2OE significantly improved spatial working memory performance and attenuated markers of cellular senescence and astrocyte reactivity in aged mice, identifying astrocyte redox homeostasis as a potential therapeutic target in cognitive aging.

MATERIALS AND METHODS

Animals

All animal procedures were approved and conducted under the guidelines of The University of Oklahoma Health Campus (OUHC) Institutional Animal Care and Use Committee. Aged C57BL/6N male mice were obtained from the National Institute on Aging colony at Charles River and group housed in conventional rodent facilities at OUHC. At euthanasia, animals were intracardially perfused with heparinized (2 units/mL) phosphate-buffered saline (1X PBS; pH 7.4) prior to tissue harvest. Hemibrains were either fixed overnight in 4% paraformaldehyde or dissected into regions of interest (hippocampus, cortex) and flash frozen for further analyses.

Astrocyte-specific SOD2 overexpression via AAV

Purified recombinant AAV(PHP.eB)-GFAP-hSOD2-P2A-GFP and AAV(PHP.eB)-GFAP-GFP expression vectors were produced by SignaGen Laboratories, formulated in sterile phosphate-buffered saline (PBS, 1X, pH 7.4) with titer determined via real time PCR. Aged mice were briefly anesthetized using isoflurane gas and administered rAAV into the right retroorbital sinus ($6x10^{11}$ vg/100µL of normal saline per injection) at 17-18 months of age. Animals were then cognitively tested following 4 months of overexpression at 21-22 months of age.

Primary astrocyte cultures

Mixed cortical and hippocampal primary astrocytes were cultured from postnatal day 1-3 C57BL/6J pups as previously reported [7, 16]. Following confluency, astrocytes were treated with either AAV(PHP.eB)-GFAP-hSOD2-P2A-GFP (AAV-SOD2) or AAV(PHP.eB)-GFAP-GFP (AAV-GFP) at a titer of $1x10^{10}$ vg/culture for five days. Following treatment, cultures were rinsed with ice cold PBS (1X, pH 7.4), scraped, and either fractionated or pelleted and flash frozen in liquid nitrogen and stored at -80°C until further analysis.

For fractionation, cells were resuspended in 1 mL of immunocapture buffer [17] containing 105 mM K-MES, 30 mM KCl, 10 mM KH_2PO_4, 5 mM $MgCl_2 \times 6H_2O$ supplemented with cOmplete Protease Inhibitor cocktail (Roche). Membranes were disrupted using a Dounce homogenizer and spun at 1,000 x g for 5 minutes to remove nuclei and debris. The supernatant was then spun at 20,000 x g for 10 minutes to pellet mitochondria. The remaining supernatant was used as the cytosolic fraction. Whole cell lysate, mitochondrial, and cytosolic fractions were then utilized for downstream immunoblotting.

SOD2 activity

SOD2 activity was quantified in whole cell lysates of primary astrocytes and in hippocampal lysates treated with AAV-GFP and AAV-SOD2 using an SOD assay kit (Cayman Chemical). Each reaction contained 10µg of

whole cell or tissue lysate in the presence of 3mM potassium cyanide to determine SOD2 activity following the generation of superoxide by xanthine oxidase. Absorbance was read at 440nm following 30min incubation following the manufacturer's instructions.

Automated home-cage spatial memory assessment (PhenoTyper)

Spatial working memory of mice was evaluated using an automated-home cage testing paradigm (PhenoTyper, Noldus) as described [7, 14, 16]. Spontaneous activity of individual mice was recorded over 90 hours with an infrared-sensitive camera using EthoVision XT 14 software (Noldus Information Technology, Wageningen, The Netherlands). The cages were transparent plastic (L x W x H = 30 x 30 x 35 cm) and bedding was cellulose-free paper (Pure-o'Cel; The Andersons, Maumee, OH). Body weights of mice were measured immediately before the initiation of the study and immediately after completing the behavioral tasks.

Mice were placed individually in the PhenoTyper for a 6-hour adaptation period and beginning at 1600 h on day 1, the activity of the animals was continuously recorded for 90 hours. All movements were recorded with an infrared-sensitive video camera above the arena using the X-Y coordinates of the center of gravity of each animal. These data were sampled at a rate of 15 frames per second (fps) and processed by Lowess smoothing using EthoVision. Water was available *ad libitum,* while pellet food (Dustless Precision Rodent Pellets, F05684, Bio-Serv, Flemington, NJ) was automatically dispensed using a FR5 schedule when mice successfully performed the task. Initial learning (hours 1-49) and reversal learning (hours 51-90) were assessed based on the performance of mice to enter the left or right entrance of the Cognition Wall, respectively. The data were exported from EthoVision as a text file and then processed using Python scripts. To assess performance, success rates for both initial and reversal learning were defined as the percent of correct entries within the trailing 30 entries to reach an 80% success rate. The Independent Leaning Index was also calculated per hour based on correct entries minus the incorrect entries divided by the total number of entries. This index was plotted cumulatively as a cumulative learning index to visualize learning progression over time. Measures of cognitive flexibility (rate of extinction and relearning during the first dark phase of the reversal) and maximal learning (cumulative performance across the entire reversal) were derived from the cumulative learning index as described [13]. Cognitive flexibility was calculated as correct entries minus incorrect entries divided by the total number of entries during the first dark phase of reversal learning between hours 51 and 61 after initiation of the experiment. Animals are removed from the study if they receive fewer than 10 pellet drops during the acquisition task or due to technical issues with pellet dispensers. This exclusion represented <10% of all mice in our study, irrespective of age. It should be noted that in this study all animals met criteria during the initial discrimination phase and thus none were excluded. Following behavior testing, all mice were returned to group housing with chow food for one week before harvesting for tissue.

Immunoblotting

Hippocampal and cortical protein lysates were prepared in RIPA buffer containing cOmplete Protease Inhibitor cocktail (Roche) and subjected to SDS-PAGE as described [7]. Briefly, equal amounts of protein (10µg/lane) underwent gel electrophoresis using a NuPAGE 4-12% Bis-Tris gel (Invitrogen), transferred to a nitrocellulose membrane, blocked in 5% BSA, and probed for targets of interest provided in Table 1.

Table 1. Antibodies used for immunoblotting.

Antibody	Dilution	Catalogue number, vendor
SOD2 (human)	1:5,000	MA1-106, Invitrogen
SOD2 (mouse)	1:2,000	Ab13533, Abcam
COX IV	1:1,000	4844, Cell Signaling
Serine racemase	1:1,000	17955-1-AP, Proteintech
Actin	1:10,000	MAB1501, Sigma-Aldrich
IRDye® 680RD Donkey anti-Mouse IgG Secondary	1:5,000	926-68072, LICORbio
IRDye® 800CW Donkey anti-Rabbit IgG Secondary	1:5,000	926-32213, LICORbio

Immunofluorescence

Standard immunofluorescent labeling of cryosectioned brain samples was performed as previously described [7, 16]. Cryopreserved sagittal sections (30µm) underwent antigen retrieval, blocked in 5% bovine serum albumin in Tris buffered saline with 0.1% Tween (TBST; pH 7.4), then incubated with appropriate primary/secondary antibodies for targets of interest provided in Table 2. Following mounting, sections were cover-slipped with Prolong Gold with DAPI, and Z-stack images were obtained using a Nikon W1CSU-SoRa spinning disk confocal microscope, and denoised/3D deconvolved using NIS-Elements AR software. The percentage of transfected astrocytes was quantified from the number of GFP-labeled astrocytes normalized to the total GFAP-labeled astrocyte count in the dentate gyrus (DG) and the

stratum radiatum (SR) regions of the hippocampus. Morphology of GFP-GFAP doubled-labeled astrocytes was then assessed via Sholl analysis using the Simple Neurite Tracer v4.2.1 plugin of FIJI-ImageJ2. A total of 30 GFP-GFAP double-labeled hippocampal astrocytes from 3-4 sections were analyzed for each animal. For more details regarding immunofluorescence methodology, please see Baier et. al, 2025 [16].

Table 2. Antibodies used for immunofluorescence.

Antibody	Dilution	Catalogue number, vendor
GFP	1:1,000	ab290, Abcam
GFAP	1:1,000	CPCA-GFAP, EnCor
Goat anti-Rabbit IgG Alexa Fluor™ 488	1:1,000	A11008, Invitrogen
Goat anti-Chicken IgY Alexa Fluor™ Plus 647	1:1,000	A32933, Invitrogen
DAPI	1:2,000	62248, Thermo

Quantitative PCR

Hippocampal RNA was extracted and processed for cDNA from equal concentrations of total RNA (1000ng) as previously described [16] using the RNeasy Mini (Qiagen) and the High-Capacity RNA-to-cDNA (Applied Biosystems) kits, respectively. Quantitative RT-PCR was performed using the gene-specific TaqMan expression assays (Applied Biosystems) provided in Table 3. PCR was performed using TaqMan Universal PCR Master Mix with UNG and the QuantStudio 12k Flex System (Applied Biosystems). Expression data were calculated using the comparative C_T method from two replicates normalized to the geometric mean of housekeeping gene expression (*Cyc1* and *Ube2d2*). Data are presented as fold changes over mean young expression.

Table 3. Primers used for qPCR.

Gene	Primer sequence/catalogue number
p16^{INK4a}	forward: 5'-AACTCTTTCGGTCG TACCCC-3' reverse: 5'-TCCTCGCAGTTCGA ATCTG-3'
p21^{WAF1} **(transcript variant 2)**	APT2FJW
Gfap	Mm01253033_m1
Serpina3n	Mm00776439_m1
H2-D1	Mm04208017_mH
Il-1b	Mm00434228_m1
Ccl2	Mm00441242_m1
Cxcl10	Mm00445235_m1
Tnf	Mm00443258_m1
Cyc1	Mm00470540_m1
Ube2d2	Mm00785931_s1

RNA-seq library preparation and sequencing

Directional libraries RNA-seq were made from total hippocampal RNA (1000ng) according to the manufacturer's protocol as previously described [18]. Poly-adenylated RNA was captured using NEBNext Poly(A) mRNA magnetic isolation module (NEB#E7490, New England Biolabs, Ipswich, MA). Following mRNA capture, mRNA was eluted from oligo-dT beads and fragmented by incubating with First Strand Synthesis reaction buffer and Random Primer Mix (2x) from the NEBNext Ultra II Directional Library Prep kit for Illumina (NEB#E7760) at 94ºC for 15 min. First and second strand cDNA synthesis was performed sequentially per the manufacturer's instructions. After purification of double-stranded cDNA with 1.8x SPRISelect beads (#B23318, Beckman Coulter), cDNA was eluted in 15 µl of 0.1x TE. cDNA libraries were then amplified with 8cycles of PCR using the NEBNext Ultra II Q5 master mix and unique index primer mixes from the NEBNext Multiplex Oligos for Illumina Library kit (#E6642S). Libraries were purified with 0.9x SPRISelect beads and then sized with HSD1000 ScreenTapes (#5067-5584, Agilent Technologies). Libraries were then quantified by Qubit 1x dsDNA HS Assay kit (#Q33230, Invitrogen). Libraries for each sample were pooled at 4 nm concentration and sequencing was performed using an Illumina NovaSeq 6000 system (S4 PE150).

RNA-seq data analysis

Following sequencing, reads were trimmed and aligned prior to downstream analyses in Strand NGS software (v4.0, Strand Life Sciences). Reads were aligned against the full mm39 genome. Alignment and filtering criteria included: adapter trimming, fixed 2-bp trim from 5' and 3' ends, a maximum number of one novel splice allowed per read, a minimum of 90% identity with the reference sequence, a maximum 5% gap, and trimming of 3' ends with Q<30. Alignment was performed directionally, with read 1 aligned in reverse and read 2 in forward orientations, respectively. All duplicate reads were then removed. Normalization was performed with DESeq2. Transcripts with an average read count value >20 in at least 100% of the samples in at least one group were considered expressed at a level sufficient for quantitation per tissue and those transcripts below this level were considered not detected/not expressed and excluded, as these low levels of reads are close to background and are highly variable. Generation of principal component plots and heatmaps, in addition to gene ontology (GO) and gene set enrichment analysis (GSEA), were performed in RStudio (build 375, R version 4.1).

Statistical analyses

All experiments were performed in multiple independent replicates per group, with statistical analyses performed using GraphPad Prism 10, JMP v15.2.0, and RStudio build 375, R version 4.1. Normality of data was assessed via Shapiro-Wilks test. For experiments with samples sizes n<6, non-parametric tests were applied. Behavioral data were analyzed using a repeated measures ANOVA (age x group x time) using JMP [14]. Molecular data comparing two groups were analyzed via student's T test or Mann-Whitney U test (non-parametric). Data with three groups were analyzed via one-way or two-way ANOVA with Šidák's multiple comparisons (parametric) or Kruskal-Wallis test with Dunn's multiple comparisons (non-parametric) tests [16]. Data are represented as mean ± SEM. Sample sizes are noted for each experiment with significance denoted as *p<0.05, **p<0.01, ***p<0.001, ****p<0.0001.

RESULTS

Viral-mediated overexpression of SOD2 in astrocytes

To overexpress human SOD2 (hSOD2) in astrocytes, we generated two recombinant AAV (rAAV) constructs: AAV(PHP.eB)-GFAP-hSOD2-P2A-eGFP (aSOD2OE) and AAV(PHP.eB)-GFAP-GFP (GFP). The PHP.eB capsid was chosen for its high blood-brain barrier penetration [19], allowing for effective transduction throughout the brain following retroorbital injection. Additionally, we used the GFAP promoter to drive expression in astrocytes in attempt to limit potential off target effects, as Aldh1l1 is expressed by multiple peripheral tissues, including liver, kidney, lung, and small intestine [20].

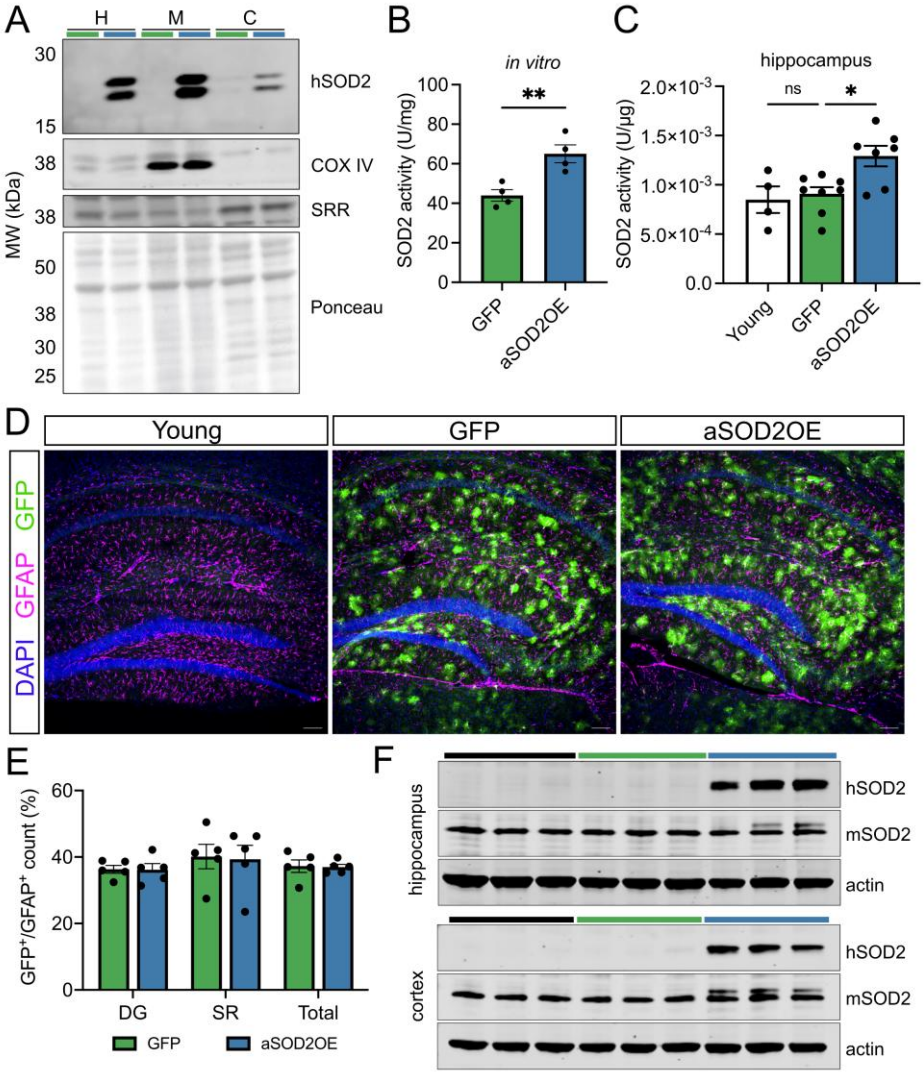

Figure 1. AAV-induced SOD2OE in astrocytes shows cell and organelle specificity *in vitro* and *in vivo*. (A) Representative immunoblot of hSOD2, COX IV (mitochondrial marker), and serine racemase (SRR; cytosolic marker) of cell homogenate (H), mitochondrial (M) and cytosolic (C) fractions of primary astrocytes treated with rAAV. Colored bars above lanes represent GFP (green) and aSOD2OE (blue) samples. **(B-C)** SOD2 activity assessed in (B) cell lysates of rAAV-treated primary astrocytes (n=4 independent cultures/group) and (C) hippocampal samples of young and aged rAAV-treated animals (n=4-8 animals/group). **(D)** Representative confocal images of hippocampal sections from young and aged rAAV-treated GFP and aSOD2OE mice. Scale bar, 100µm. **(E)** Proportion of GFP-labeled astrocytes normalized to the total GFAP-labeled astrocyte count in the dentate gyrus (DG) and the stratum radiatum (SR) regions of the hippocampus. n=5 animals/group. **(F)** Representative immunoblot of hSOD2, endogenous mouse SOD2 (mSOD2) in young and rAAV-treated aged mice. Colored bars above lanes represent young (black), aged GFP (green), and aged aSOD2OE (blue) samples. For all graphs, colors represent the following: young (black), GFP (green), aSOD2OE (blue). Error bars: mean ± SEM. *p<0.05, **p<0.01.

We validated our rAAVs using both *in vitro* and *in vivo* approaches. Following treatment of rAAV in primary astrocyte cultures, we confirmed overexpression of hSOD2 in fractionated cell lysates that localized mainly within the mitochondrial fraction (Fig. 1A), denoted by organelle-specific expression of COX IV. SOD2OE astrocytes mirrored an increase in SOD2 activity compared to GFP controls, thereby validating the functionality of the hSOD2 construct (Fig. 1B).

In vivo, aged aSOD2OE animals showed similar increases in SOD2 activity in the hippocampus compared to young and GFP-treated aged animals (Fig. 1C). Using histological methods, we confirmed widespread expression of GFP colocalizing with GFAP-immunolabeled astrocytes throughout the brain (e.g., hippocampus, Fig. 1D). Quantification of transduction efficiency in the DG and SR regions of the hippocampus revealed an approximate total efficiency of 40% in both GFP and aSOD2OE treated aged mice (Fig. 1E). Immunoblotting of hippocampus and cortex samples from young and rAAV-treated aged mice showed expression of hSOD2, with no alterations in endogenous mouse SOD2 (mSOD2) levels between aged groups (Fig. 1F). Consistent with reports of extra-neural GFAP expression by hepatic stellate cells [21], we did note peripheral hSOD2 expression in liver, but not in other peripheral tissues (e.g., quadriceps), illustrating specificity of the GFAP-driven hSOD2 expression (Supplementary Fig. 1).

Enhancing astrocyte antioxidant capacity improves age-related spatial working deficits

To assess the impact of enhancing astrocyte mitochondrial antioxidant capacity on age-associated cognitive decline, we induced overexpression of hSOD2 utilizing our recombinant AAV(PHP.eB)-GFAP constructs. Our experimental cohort of aged C57BL/6N mice were administered either AAV(PHP.eB)-GFAP-hSOD2-P2A-eGFP (aSOD2OE) or AAV(PHP.eB)-GFAP-GFP (GFP) to serve as aged controls via retroorbital injection at 18 months of age.

Following four months of overexpression, spatial working memory of aged GFP and aSOD2OE mice was assessed at 22 months of age in a home-cage testing platform (PhenoTyper) using established protocols [7, 14, 16]. Following placement in the home cage, initial and reversal learning was assessed over 90 hours of testing based on the ability of mice to enter one of three holes for a food reward. Performance in the initial and reversal phases were assessed for each hour and visualized as a cumulative learning index, depicting the ratio of efficiency of correct entries to the total entries compounded over the duration of each respective phase (Fig. 2A). Additional metrics used for evaluation of spatial working memory included the number of entries required to reach an 80% success rate (entries to 80% criterion), cognitive flexibility (rate of extinction and re-learning during the reversal), and maximal learning (cumulative performance in the reversal).

Aged GFP and aSOD2OE animals performed comparably in the initial learning phase, with all mice in both groups reaching criterion in a similar number of entries (Fig. 2B). Age-related increases in the number of entries to reach criterion in the reversal were noted, with total of 29% of GFP and 16% of aSOD2OE mice failing to reach criterion. While both groups showed similar performance in the initial phase (Fig. 2C), aged aSOD2OE mice showed significantly higher cognitive flexibility (Fig. 2D) and maximal learning (Fig. 2E) compared to aged GFP controls.

Age-related cognitive decline has been associated with alterations in mitochondrial energy metabolism and redox signaling [22-24]. We have previously shown that SOD2-KO in astrocytes increased oxidative damage marker, 3-nitrotyrosine (3-NT), in the hippocampus that correlated with decreased spatial memory performance [7]. Therefore, we assessed whether aSOD2OE has an impact on 3-NT levels in aged mice. Levels of 3-NT were significantly reduced with aSOD2OE compared to GFP

controls (Supplementary Fig. 2), suggesting a direct interaction of astrocyte SOD2 expression on hippocampal oxidative stress. To determine whether the beneficial effects on cognition with aSOD2OE is mediated in part through improved mitochondrial respiration, we conducted high-resolution respirometry (Oroboros instruments) in the hippocampus [14, 25]. No differences were noted in oxygen consumption rate between groups across metabolic substrates and electron transport chain complex inhibitors (Supplementary Fig. 3). These data suggest that enhancement of astrocyte-specific mitochondrial antioxidant capacity was sufficient to attenuate oxidative damage and age-related declines in spatial working memory without altering overall metabolic capacity in the hippocampus.

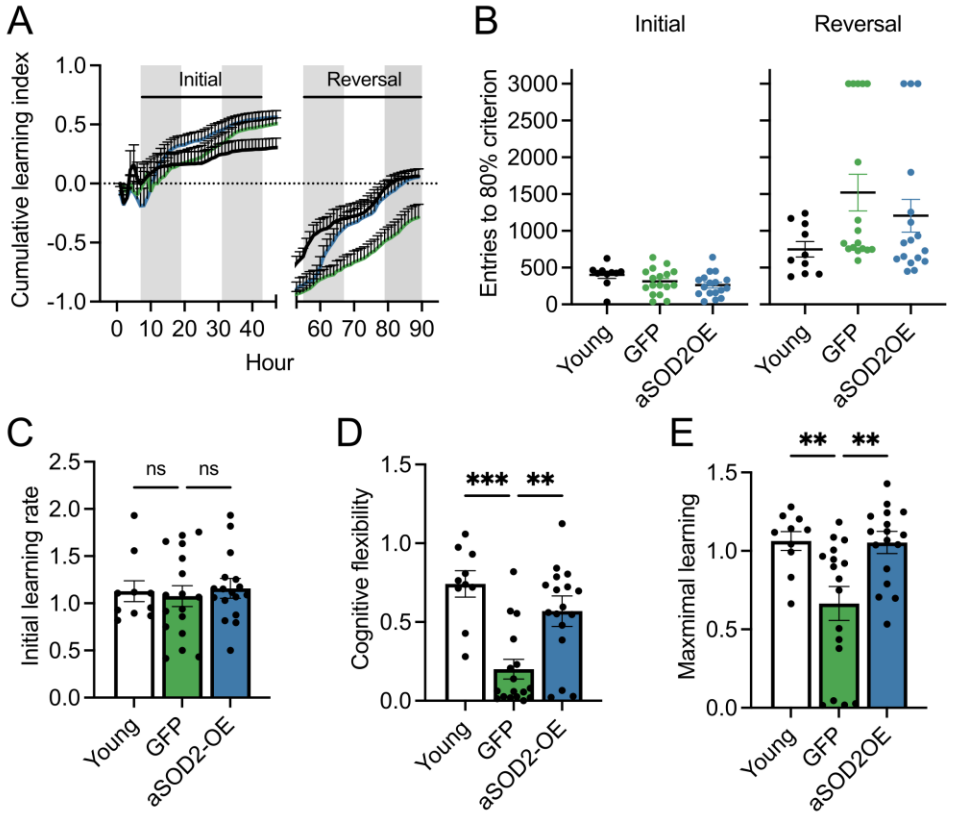

Figure 2. Age-related deficits in spatial working memory are attenuated with aSOD2OE. (A) Cumulative learning index demonstrating improved performance during the reversal phase in aSOD2OE mice. **(B)** Entries to reach 80% criterion for initial and reversal learning phases showed no significant differences between young and rAAV-treated aged mice. **(C)** Initial learning rate (derived from first dark phase of the initial phase) showed no significant differences between young and rAAV-treated aged mice. **(D-E)** Age-related deficits in cognitive flexibility (derived from first dark phase of the reversal learning phase) and maximal learning (derived from the cumulative learning index at the end of the reversal phase) were ameliorated in aSOD2OE treated mice. For all graphs, colors represent the following: young (black, n=10), aged GFP (green, n=17), aged aSOD2OE (blue, n=17). Shaded bars in graph A represent dark periods of the day/light cycle. Error bars: mean ± SEM. **p<0.01, ***p<0.001.

aSOD2OE had modest effects on the hippocampal transcriptome

To assess putative mechanisms contributing to improved spatial working memory following astrocyte-specific SOD2OE in aged animals, we performed bulk RNA-sequencing (RNA-seq) on hippocampal tissues.

Principal component analysis (PCA) of bulk transcriptomic profiles revealed robust separation of young animals from both aged groups, consistent with transcriptional profile shifts associated with age (Fig. 3A, Supplementary Fig. 4). In contrast, aged-GFP and aSOD2OE mice displayed partially overlapping transcriptomic profiles, suggesting that aSOD2OE induced subtler transcriptomic effects compared to aging alone.

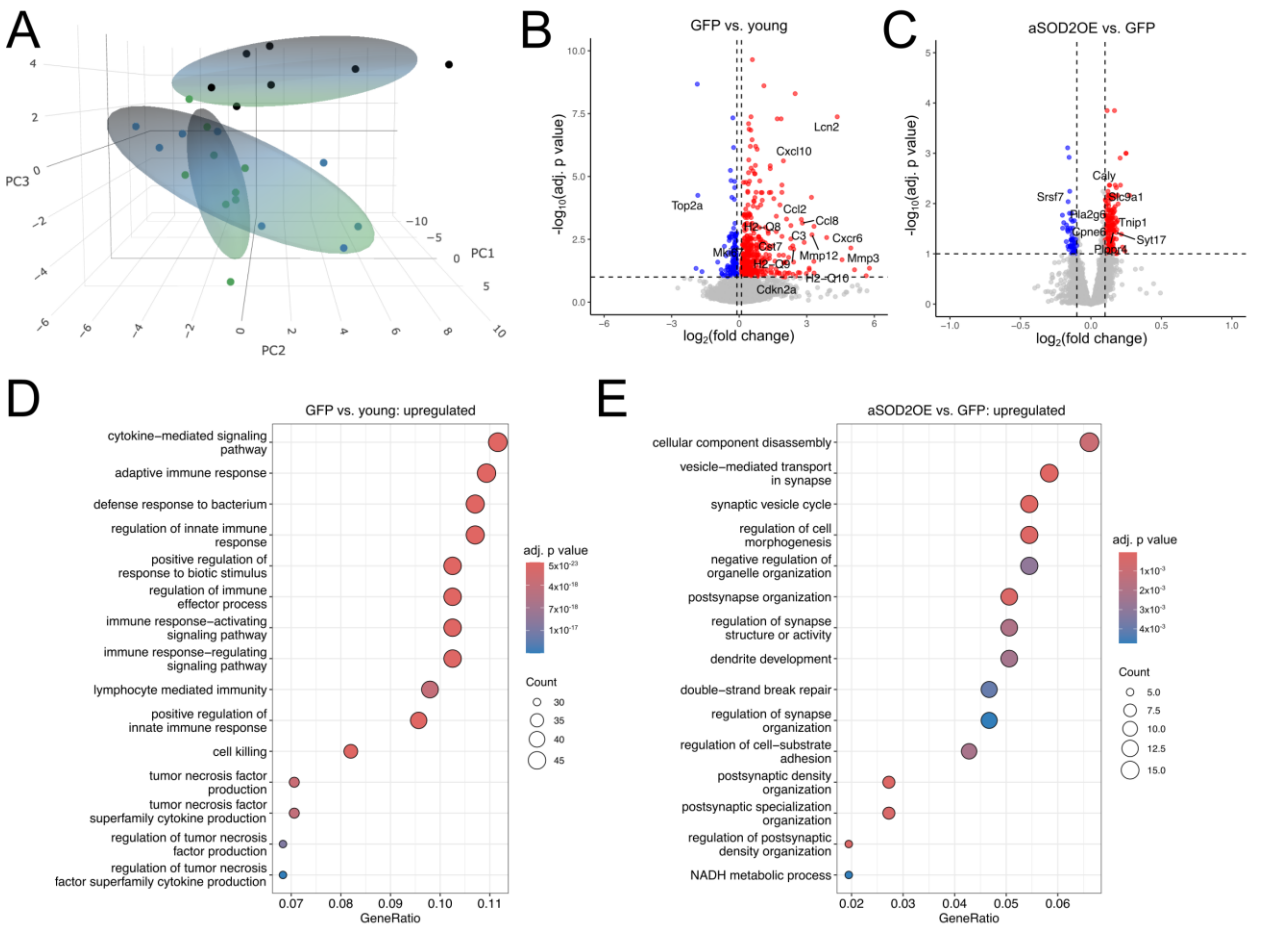

Figure 3. aSOD2OE modestly shifts the hippocampal transcriptome towards increased synaptic maintenance and reduced inflammation. (A) 3D principal component plot of PC1-PC3 depicting partial overlap of gene expression between aged aSOD2OE and GFP mice. **(B-C)** Volcano plot depicting significantly upregulated (red) and downregulated (blue) genes between (B) aged GFP and young and (C) aSOD2OE vs. GFP comparisons. **(D-E)** Dot plot depicting gene ontology biological process terms enriched in the (D) GFP vs. young and (E) aSOD2OE vs. GFP comparisons. For all RNA-seq experiments, n=7 young, 9 aged GFP, and 8 aged aSOD2OE mice, respectively.

Differential gene expression analysis between GFP and young animals showed robust upregulation of genes associated with inflammation, immune activation, and extracellular matrix remodeling, including chemokines (e.g., *Cxcl10*, *Ccl2*, *Ccl8*), complement components (*C3*), components of MHC class I (*H2-Q8*, *H2-Q9*, *H2-Q10*), and matrix metalloproteases (*Mmp3*, *Mmp12*) (Fig. 3B). Gene ontology (GO) analyses of genes upregulated in aged-GFP mice showed enrichment for immune-related pathways, including cytokine-mediated signaling, adaptive immune response, and regulation of innate immune processes (Fig. 3D), consistent with age-associated neuroinflammation.

In contrast, the comparison between aSOD2OE and aged-GFP mice revealed that most changes in expression were modest in magnitude (e.g., $|\log_2 FC| < 0.5$) (Fig. 3C). GO terms upregulated in aSOD2OE mice compared to GFP controls were associated with synaptic structure and function, including synaptic vesicle cycling, post synapse organization, regulation of synapse structure or activity, and dendrite development (Fig. 3E). Among the genes driving these enrichments were multiple synaptic-associated genes (e.g., *Syt17, Slc9a1, Plppr4*) and *Tnip1*, a negative regulator of NF-kB signaling (Fig. 3C). While individual fold changes were modest, their concerted upregulation may support the notion that aSOD2OE benefits spatial working memory by sustaining synaptic support functions and reducing inflammation within the hippocampus.

Improving astrocyte antioxidant capacity mitigates reactive astrogliosis and senescence burden in the aged hippocampus

We have previously reported that aged animals with spatial working memory impairments showed increased

burden of hippocampal cellular senescence and reactive astrogliosis [16], cellular changes that have been thought to contribute to neuroinflammation and alterations in synaptic function with age. Furthermore, we and others have shown that the ablation of SOD2 in astrocytes impairs spatial working memory [7] with a concomitant increases reactive astrogliosis in the brain [7, 8]. We therefore assessed whether age-associated reactive astrogliosis was altered with astrocyte SOD2 overexpression by histological and molecular approaches.

To assess astrocyte morphology, we analyzed high-magnification confocal images of GFAP immunolabeled astrocytes colocalizing GFP within the CA1 region of the hippocampus using Sholl analysis (Fig. 4A-D). Quantification revealed decreases in the maximal number of intersections and the maximal branch length of GFAP-GFP double-labeled astrocytes in aSOD2OE mice compared to GFP controls. Consistent with decreased astrocyte arborization assessed by Sholl analysis, *Gfap* transcript expression was decreased in the hippocampus of aSOD2OE mice compared to aged GFP controls. Similarly, transcripts associated with reactive astrocyte phenotypes (e.g., *Serpina3n*, *H2-D1*) that were elevated with age were significantly decreased in the aSOD2OE hippocampus (Fig. 4E).

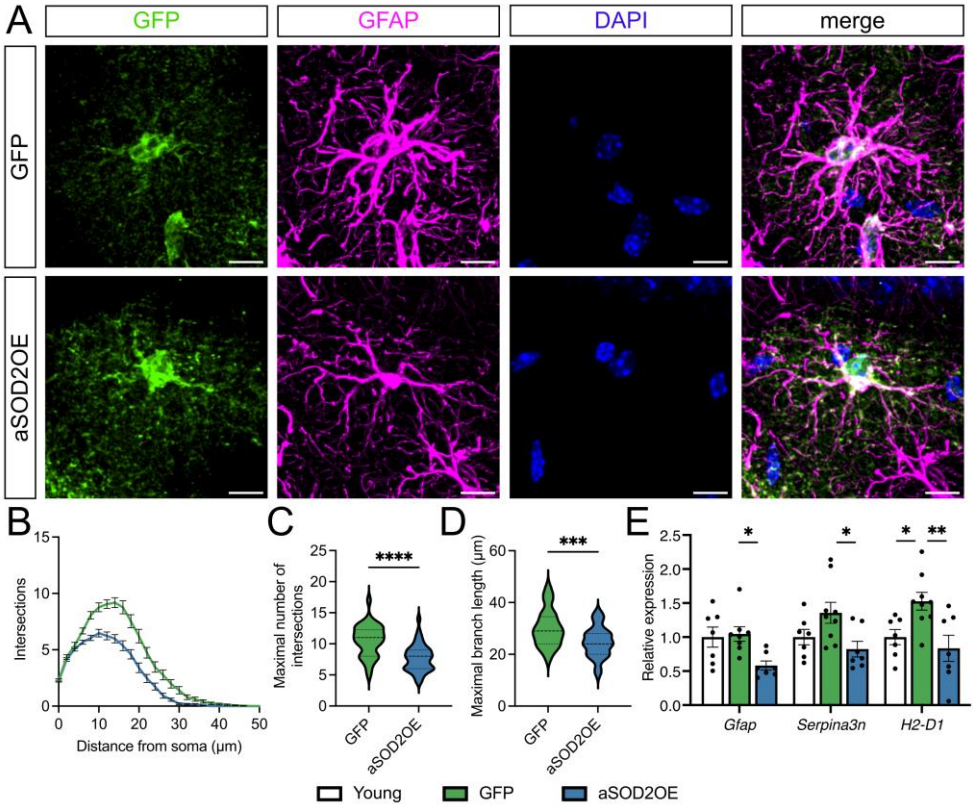

Fig. 4. Age-related increases in reactive gliosis are attenuated with aSOD2OE. (A) Representative confocal images of individual astrocytes with the CA1 region of hippocampal sections immunolabeled for GFP (green), GFAP (pink; astrocytes), and DAPI (blue; nuclei). Scale bar, 10μm. **(B)** Quantification of the number of astrocyte projections plotted against the radial distance from the soma of GFP$^+$-GFAP$^+$ double-labeled astrocytes obtained via Sholl analysis. n=30 astrocytes/animal, 3-4 sections per animal, n=5 mice/group. **(C-D)** Maximal branch length and maximal number of intersections of GFP$^+$-GFAP$^+$ double-labeled astrocytes quantified using Sholl analysis. n=30 astrocytes/animal, 3-4 sections per animal, n=5 mice/group. **(E)** Transcriptional expression of astrocyte reactivity markers (*Gfap*, *Serpina3n, H2-D1*) within the hippocampus. n=7-9 mice/group. For all graphs, colors represent the following: young (black), aged GFP (green), aged aSOD2OE (blue). Error bars: mean ± SEM. *p<0.05, **p<0.01, ***p<0.001, ****p<0.0001.

Given the observed reductions in astrocyte reactivity in aSOD2OE mice, we next sought to determine whether SOD2 levels directly influence astrocyte senescence. Specifically, we examined whether loss of SOD2 was sufficient to induce senescence-associated phenotypes in astrocytes. To do this, we established primary astrocyte cultures from *Sod2$^{f/f}$* pups and ablated SOD2 using AAV1-CRE [7]. Following five days of ablation, we

assessed gene expression of canonical markers of cellular senescence, including cyclin-dependent kinase inhibitors (e.g., *p16*^{INK4a}, *p21*^{WAF1}) and pro-inflammatory senescence-associated secretory phenotype factors (*Il-6*, *Ccl2*, *Cxcl1*, *Cxcl10*, *Mmp3*). Compared to controls, SOD2-deficient astrocytes exhibited robust upregulation of both cell-cycle arrest markers and SASP factors (Fig. 5A-B), further supporting a cell-autonomous role for SOD2 in inducing astrocyte senescence when dysregulated.

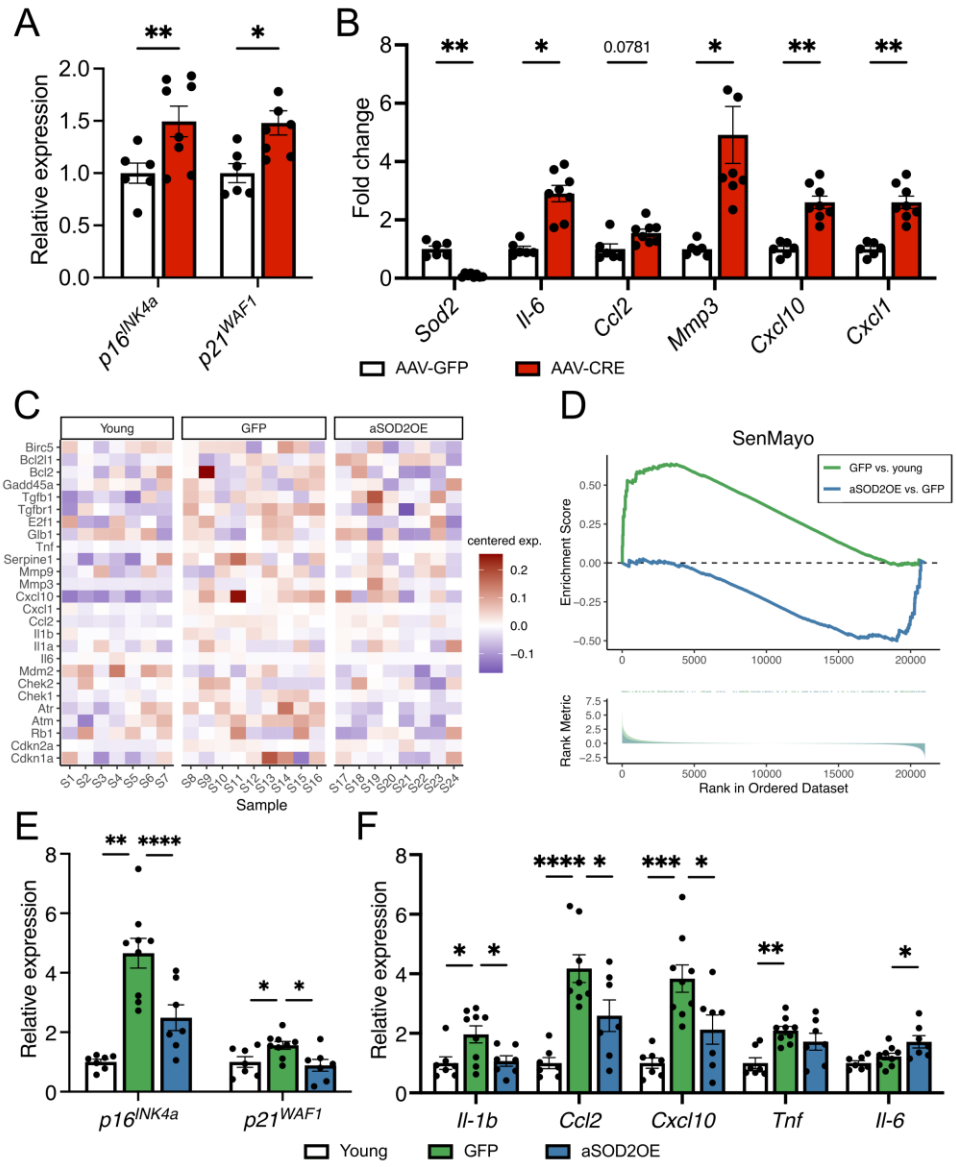

Figure 5. aSOD2OE attenuates age-associated increases in hippocampal cellular senescence gene expression. (A-B) Transcriptional expression of cyclin-dependent kinase inhibitors (*p16*^{INK4a}, *p21*^{WAF1}) and SASP factors (*Il-6*, *Ccl2*, *Mmp3*, *Cxcl10*, *Cxcl1*) associated with senescence were increased following Cre-mediated ablation of *Sod2 in vitro*. n=6-8 independent cultures/group. **(C)** Heatmap of senescence-associated genes from RNA-seq. **(D)** GSEA plot demonstrating enrichment scores of the SenMayo gene set panel. **(E-F)** Transcriptional expression of cyclin-dependent kinase inhibitors (*p16*^{INK4a}, *p21*^{WAF1}) and SASP factors (*Il-1b*, *Ccl2*, *Cxcl10*, *Tnf*) increased within the hippocampus with age were attenuated with aSOD2OE. For graphs A-B, colors represent the following: AAV-GFP (white), AAV-CRE (red). For graphs E-F, colors represent the following: young (black, n=7), aged GFP (green, n=9), aged aSOD2OE (blue, n=8). Error bars: mean ± SEM. *p<0.05, **p<0.01, ***p<0.001, ****p<0.0001.

These findings suggested that enhancing aSOD2OE *in vivo* may attenuate age-associated senescence burden in the brain. To assess whether aSOD2OE may attenuate brain senescence burden in aging, we assessed senescence-associated markers in our hippocampal RNA-seq data from aged mice (Fig. 5C). We performed gene set enrichment analysis (GSEA) using the SenMayo senescence gene set [26]. The enrichment in SenMayo in aged-GFP mice compared to young mice (NES = 1.582, p.adjust = 7.13 x 10^{-4}) was significantly downregulated in aSOD2OE mice compared to GFP controls (NES =-1.425, p.adjust = 1.458 x 10^{-2}) (Fig. 5D).

To validate our RNA-seq findings, we assessed expression of cell cycle arrest markers ($p16^{INK4a}$, $p21^{WAF1}$) and SASP factors (*Il-1b*, *Ccl2*, *Cxcl10*, *Tnf*) via qPCR. Consistent with downregulation of the SenMayo panel, aSOD2OE mice showed decreased gene expression of both cyclin-dependent kinase inhibitors (Fig. 5E) and SASP factors (Fig. 5F), suggesting that improving astrocyte mitochondrial antioxidant capacity may be sufficient to attenuate brain senescence burden with age.

Collectively, these findings demonstrate that augmenting astrocyte antioxidant capacity with SOD2 overexpression mitigates key hallmarks of brain aging, namely cellular senescence and neuroinflammation, while concomitantly reducing impairments in spatial memory performance in aged mice. This supports a model in which astrocyte-specific antioxidant capacity is integral to preventing induction of cellular senescence and preserving cognitive function in the aging brain.

DISCUSSION

Astrocytes are increasingly recognized as central regulators of brain aging, owing largely to their roles in maintaining synaptic function, metabolic homeostasis, and redox balance [27]. Given the high energetic demands of neurons and large quantities of ROS generated through oxidative phosphorylation, astrocytes serve as essential providers of antioxidant support (e.g., glutathione and its amino acid precursors [28]) to the neural milieu [29].

In response to CNS insults, astrocytes undergo reactive astrogliosis, a collection of morphological and functional alterations, contributing to synaptic dysfunction and increased secretion of pro-inflammatory effectors by astrocytes [30]. During normative aging, astrocytes undergo polarization to a neurotoxic reactive astrocyte phenotype, concomitant with reduced antioxidant gene expression [4]. Among antioxidant enzymes, SOD2 represents a key mitochondrial matrix antioxidant responsible for the conversion of superoxide to hydrogen peroxide. Previously, we [7] and others [8] have shown that astrocyte-specific ablation of SOD2 in middle/late age resulted in spatial working memory deficits, downregulation of mitochondrial OXPHOS genes, and increased markers of cellular senescence and reactive astrogliosis. These findings motivated our current study into whether enhancing SOD2 expression in astrocytes could mitigate cognitive deficits and cellular hallmarks associated with aging.

Here, we report that aSOD2OE resulted in significant improvements in hippocampal spatial working memory compared to aged GFP controls. These findings align with and expand upon prior work in pathological settings, where overexpression of SOD2 (cell type agnostic) in the brain protected against AD-like cognitive deficits in the Tg2576 AD mouse model [31] and astrocyte-specific overexpression of SOD2 in the hippocampus reduced CA1 neuronal vulnerability to forebrain ischemia [32]. Interestingly, aSOD2OE did not alter hippocampal mitochondrial respiration, which aligns with prior reports showing no change in basal metabolism in brain, liver and muscle with hSOD2 overexpression [33]. Furthermore, transgenic overexpression of SOD2 increased cardiac function despite no change in respiratory control index (ratio of State 3 to State 4) compared to controls [34]. Together, these results provide evidence that despite no overall changes in tissue respiration, enhancement to astrocyte antioxidant capacity provides functional benefits to cognitive function across aging and pathological contexts.

Increased ROS and damage to macromolecules, including DNA, protein, and lipids [9], are interconnected hallmarks of aging that contribute to the induction of cellular senescence [1]. Genetic ablations of SOD2 have been previously shown to induce DNA damage, triggering the DNA damage response and inducing cellular senescence in brain [8] and peripheral tissues [15]. Moreover, brain- and astrocyte-specific SOD2 knockout mice have been shown to have increased reactive astrogliosis [7, 8, 35]. Given the reduction of SOD2 activity [36] and transcriptional expression in the brain [7] by 18 months of age, we investigated whether overexpression of SOD2 in astrocytes protected against the age-related burden of senescent cells and reactive astrogliosis in the brain. Concomitant with benefits in spatial working memory, we found that aSOD2OE significantly reduced molecular signatures of cellular senescence and reactive astrogliosis within the hippocampus. In light of our work demonstrating increased burden of cellular senescence and reactive astrogliosis in the hippocampus of cognitively stratified aged mice [37], these data posit astrocyte antioxidant capacity as one possible mechanism contributing to brain senescence burden and associated detriments to brain function.

ROS is frequently attributed towards playing negative roles in aging and neurodegenerative diseases.

Conversely, reductions in oxidative stress with antioxidant supplementation shown to have varying efficacy in preclinical models (reviewed by [38]). While ROS can be detrimental in settings of oxidative damage, recent work has highlighted particularly the role of H_2O_2 as a key signaling molecule for brain function. In astrocytes, H_2O_2 signaling in low levels confers protection against oxidative stress in part through Nrf2-mediated biosynthesis and release of glutathione [39, 40]. Astrocytes, while historically viewed as predominantly glycolytic, rely on intact mitochondrial function (including OXPHOS and fatty acid oxidation) to support brain function [41] and maintain redox signaling. Compared to neurons, astrocytes produce more ROS due to the increased proportion of free complex I [42], with recent studies highlighting the role of fatty acid oxidation in maintaining this energetically inefficient conformation to maintain redox signaling [43]. Astrocyte-derived H_2O_2 supports long-term memory formation in Drosophila [44], whereas modulation of astrocyte H_2O_2 via mitochondrially-targeted catalase resulted in neuronal structure impairments and deficits in short-term memory [45]. Given these data, it is plausible that in addition to reducing oxidative damage, increasing H_2O_2 abundance from aSOD2OE may be mediating some of the functional benefits to cognition, which warrants further investigation.

In our study, we acknowledge several potential limitations. First, this study does not consider potential sexual dimorphisms of aSOD2OE as only male mice were used. Additionally, use of GFAP may not be reflective of the full astrocyte population, whereas Aldh1l1 is commonly recognized as a pan-astrocyte marker [46]. GFAP is one marker of reactive astrocytes that show declines in antioxidant gene expression with age [4], however. Additionally, we recognize that Aldh1l1 expression extends to multiple peripheral organs (e.g., lung, liver, kidney, small intestine) [20]. Hence, considering all options, we utilized GFAP-driven overexpression of SOD2 to limit off-target, confounding peripheral effects on cognitive function. Despite this, the effect of SOD2OE in non-neural GFAP-expressing cells (e.g., stellate cells in the liver) may provide a potential confound to our findings. Additionally, bulk RNA-sequencing of hippocampal tissue lacks resolution in discerning cell-type specific responses, which may obscure subtle changes in effected cells.

In sum, our findings contribute new evidence that enhancing astrocyte antioxidant capacity is a central player in alleviating cellular hallmarks of maladaptive aging to preserve cognitive function. As accumulating evidence suggests alterations in astrocytes as drivers of age- and neurodegenerative disease-associated cognitive dysfunction, modulating astrocytic redox biology may offer a promising therapeutic avenue to maintain brain function in aging.

Acknowledgements

We thank the Oklahoma Nathan Shock Center Genomic Sciences Core (Dr. Willard Freeman and Kevin Pham) for assistance in RNA-seq library preparation and alignment of sequencing data.

This research was supported by the following funding sources: National Institute on Aging (NIA) T32AG 052363 (MPB), R00AG056662 (SL), R01AG085398 (SL). This research was also supported by NIGMS: the Molecular Analysis Cellular Imaging and Animal Model Development and Behavioral Assessment cores of the "Cellular and Molecular GeroScience CoBRE" (P20GM125528).

Author's Contributions

MPB and SL designed the study. MPB, SS, JW, SN, and CN performed research. MPB, SIS and SL analyzed data. MPB and SL wrote the paper. All authors read and approved the final version of the paper.

Data and materials availability

Data may be made available on reasonable request to the corresponding author. Correspondence and requests for information should be addressed to SL.

Supplementary Materials

The Supplementary data can be found online at: www.aginganddisease.org/EN/10.14336/AD.2025.0760.

References

[1] López-Otín C, Blasco MA, Partridge L, Serrano M, Kroemer G (2013). The hallmarks of aging. Cell, 153:1194-1217.

[2] Bolaños JP (2016). Bioenergetics and redox adaptations of astrocytes to neuronal activity. J Neurochem, 139 Suppl 2:115-125.

[3] McBean GJ (2018). Astrocyte Antioxidant Systems. Antioxidants (Basel), 7.

[4] Clarke LE, Liddelow SA, Chakraborty C, Münch AE, Heiman M, Barres BA (2018). Normal aging induces A1-like astrocyte reactivity. Proc Natl Acad Sci U S A, 115:E1896-e1905.

[5] Chen Y, Qin C, Huang J, Tang X, Liu C, Huang K, et al. (2020). The role of astrocytes in oxidative stress of central nervous system: A mixed blessing. Cell Prolif, 53:e12781.

[6] Sasaki T, Unno K, Tahara S, Shimada A, Chiba Y, Hoshino M, et al. (2008). Age-related increase of superoxide generation in the brains of mammals and birds. Aging Cell, 7:459-469.

[7] Baier MP, Nagaraja RY, Yarbrough HP, Owen DB, Masingale AM, Ranjit R, et al. (2022). Selective Ablation of Sod2 in Astrocytes Induces Sex-Specific Effects on Cognitive Function, d-Serine Availability, and Astrogliosis. J Neurosci, 42:5992-6006.

[8] Tsesmelis K, Maity-Kumar G, Croner D, Sprissler J, Tsesmelis M, Hein T, et al. (2023). Accelerated aging in mice with astrocytic redox imbalance as a consequence of SOD2 deletion. Aging Cell, 22:e13911.

[9] Wiley CD, Campisi J (2021). The metabolic roots of senescence: mechanisms and opportunities for intervention. Nat Metab, 3:1290-1301.

[10] Ogrodnik M, Evans SA, Fielder E, Victorelli S, Kruger P, Salmonowicz H, et al. (2021). Whole-body senescent cell clearance alleviates age-related brain inflammation and cognitive impairment in mice. Aging Cell, 20:e13296.

[11] Zhang P, Kishimoto Y, Grammatikakis I, Gottimukkala K, Cutler RG, Zhang S, et al. (2019). Senolytic therapy alleviates Aβ-associated oligodendrocyte progenitor cell senescence and cognitive deficits in an Alzheimer's disease model. Nature Neuroscience, 22:719-728.

[12] Matsudaira T, Nakano S, Konishi Y, Kawamoto S, Uemura K, Kondo T, et al. (2023). Cellular senescence in white matter microglia is induced during ageing in mice and exacerbates the neuroinflammatory phenotype. Communications Biology, 6:665.

[13] Baier MP, Ranjit R, Owen DB, Wilson JL, Stiles MA, Masingale AM, et al. (2025). Cellular Senescence Is a Central Driver of Cognitive Disparities in Aging. Aging Cell, 24:e70041.

[14] Logan S, Baier MP, Owen DB, Peasari J, Jones KL, Ranjit R, et al. (2023). Cognitive heterogeneity reveals molecular signatures of age-related impairment. PNAS Nexus, 2:pgad101.

[15] Velarde MC, Flynn JM, Day NU, Melov S, Campisi J (2012). Mitochondrial oxidative stress caused by Sod2 deficiency promotes cellular senescence and aging phenotypes in the skin. Aging (Albany NY), 4:3-12.

[16] Baier MP, Ranjit R, Owen DB, Wilson JL, Stiles MA, Masingale AM, et al. Cellular Senescence Is a Central Driver of Cognitive Disparities in Aging. Aging Cell, n/a:e70041.

[17] Fecher C, Trovo L, Muller SA, Snaidero N, Wettmarshausen J, Heink S, et al. (2019). Cell-type-specific profiling of brain mitochondria reveals functional and molecular diversity. Nat Neurosci, 22:1731-1742.

[18] Ocañas SR, Pham KD, Blankenship HE, Machalinski AH, Chucair-Elliott AJ, Freeman WM (2022). Minimizing the Ex Vivo Confounds of Cell-Isolation Techniques on Transcriptomic and Translatomic Profiles of Purified Microglia. eNeuro, 9.

[19] Chan KY, Jang MJ, Yoo BB, Greenbaum A, Ravi N, Wu WL, et al. (2017). Engineered AAVs for efficient noninvasive gene delivery to the central and peripheral nervous systems. Nat Neurosci, 20:1172-1179.

[20] Winchenbach J, Düking T, Berghoff SA, Stumpf SK, Hülsmann S, Nave KA, et al. (2016). Inducible targeting of CNS astrocytes in Aldh1l1-CreERT2 BAC transgenic mice. F1000Res, 5:2934.

[21] Gard AL, White FP, Dutton GR (1985). Extra-neural glial fibrillary acidic protein (GFAP) immunoreactivity in perisinusoidal stellate cells of rat liver. Journal of Neuroimmunology, 8:359-375.

[22] Yin F, Boveris A, Cadenas E (2014). Mitochondrial energy metabolism and redox signaling in brain aging and neurodegeneration. Antioxid Redox Signal, 20:353-371.

[23] Vancova O, Baciak L, Kasparova S, Kucharska J, Palacios HH, Horecky J, et al. (2010). In vivo and in vitro assessment of brain bioenergetics in aging rats. J Cell Mol Med, 14:2667-2674.

[24] Poon HF, Calabrese V, Scapagnini G, Butterfield DA (2004). Free radicals and brain aging. Clin Geriatr Med, 20:329-359.

[25] Logan S, Ranjit R, Rose H, Bredegaard A, Diaz-Garcia CM (2024). Simultaneous quantitative respirometry and fluorometric assays in dissected hippocampal tissue from mice. STAR Protoc, 5:102988.

[26] Saul D, Kosinsky RL, Atkinson EJ, Doolittle ML, Zhang X, LeBrasseur NK, et al. (2022). A new gene set identifies senescent cells and predicts senescence-associated pathways across tissues. Nat Commun, 13:4827.

[27] Labarta-Bajo L, Allen NJ (2025). Astrocytes in aging. Neuron, 113:109-126.

[28] Dringen R, Arend C (2025). Glutathione Metabolism of the Brain-The Role of Astrocytes. J Neurochem, 169:e70073.

[29] Baxter PS, Hardingham GE (2016). Adaptive regulation of the brain's antioxidant defences by neurons and astrocytes. Free Radic Biol Med, 100:147-152.

[30] Escartin C, Galea E, Lakatos A, O'Callaghan JP, Petzold GC, Serrano-Pozo A, et al. (2021). Reactive astrocyte nomenclature, definitions, and future directions. Nature Neuroscience, 24:312-325.

[31] Massaad CA, Washington TM, Pautler RG, Klann E (2009). Overexpression of SOD-2 reduces hippocampal superoxide and prevents memory deficits in a mouse model of Alzheimer's disease. Proc Natl Acad Sci U S A, 106:13576-13581.

[32] Xu L, Emery JF, Ouyang YB, Voloboueva LA, Giffard RG (2010). Astrocyte targeted overexpression of Hsp72 or SOD2 reduces neuronal vulnerability to forebrain ischemia. Glia, 58:1042-1049.

[33] Silva JP, Shabalina IG, Dufour E, Petrovic N, Backlund EC, Hultenby K, et al. (2005). SOD2 overexpression: enhanced mitochondrial tolerance but absence of effect on UCP activity. Embo j, 24:4061-4070.

[34] Kang PT, Chen CL, Ohanyan V, Luther DJ, Meszaros JG, Chilian WM, et al. (2015). Overexpressing

superoxide dismutase 2 induces a supernormal cardiac function by enhancing redox-dependent mitochondrial function and metabolic dilation. J Mol Cell Cardiol, 88:14-28.

[35] Izuo N, Nojiri H, Uchiyama S, Noda Y, Kawakami S, Kojima S, et al. (2015). Brain-Specific Superoxide Dismutase 2 Deficiency Causes Perinatal Death with Spongiform Encephalopathy in Mice. Oxid Med Cell Longev, 2015:238914.

[36] Cardozo-Pelaez F, Song S, Parthasarathy A, Hazzi C, Naidu K, Sanchez-Ramos J (1999). Oxidative DNA damage in the aging mouse brain. Movement Disorders, 14:972-980.

[37] Baier MP, Ranjit R, Owen DB, Wilson JL, Stiles MA, Masingale AM, et al. (2025). Cellular Senescence Is a Central Driver of Cognitive Disparities in Aging. Aging Cell:e70041.

[38] Ionescu-Tucker A, Cotman CW (2021). Emerging roles of oxidative stress in brain aging and Alzheimer's disease. Neurobiology of Aging, 107:86-95.

[39] Haskew-Layton RE, Payappilly JB, Smirnova NA, Ma TC, Chan KK, Murphy TH, et al. (2010). Controlled enzymatic production of astrocytic hydrogen peroxide protects neurons from oxidative stress via an Nrf2-independent pathway. Proc Natl Acad Sci U S A, 107:17385-17390.

[40] Shih AY, Johnson DA, Wong G, Kraft AD, Jiang L, Erb H, et al. (2003). Coordinate Regulation of Glutathione Biosynthesis and Release by Nrf2-Expressing Glia Potently Protects Neurons from Oxidative Stress. The Journal of Neuroscience, 23:3394-3406.

[41] Mi Y, Qi G, Vitali F, Shang Y, Raikes AC, Wang T, et al. (2023). Loss of fatty acid degradation by astrocytic mitochondria triggers neuroinflammation and neurodegeneration. Nat Metab, 5:445-465.

[42] Lopez-Fabuel I, Le Douce J, Logan A, James AM, Bonvento G, Murphy MP, et al. (2016). Complex I assembly into supercomplexes determines differential mitochondrial ROS production in neurons and astrocytes. Proc Natl Acad Sci U S A, 113:13063-13068.

[43] Morant-Ferrando B, Jimenez-Blasco D, Alonso-Batan P, Agulla J, Lapresa R, Garcia-Rodriguez D, et al. (2023). Fatty acid oxidation organizes mitochondrial supercomplexes to sustain astrocytic ROS and cognition. Nature Metabolism, 5:1290-1302.

[44] Rabah Y, Berwick J-P, Sagar N, Pasquer L, Plaçais P-Y, Preat T (2025). Astrocyte-to-neuron H2O2 signalling supports long-term memory formation in Drosophila and is impaired in an Alzheimer's disease model. Nature Metabolism, 7:321-335.

[45] Vicente-Gutierrez C, Bonora N, Bobo-Jimenez V, Jimenez-Blasco D, Lopez-Fabuel I, Fernandez E, et al. (2019). Astrocytic mitochondrial ROS modulate brain metabolism and mouse behaviour. Nat Metab, 1:201-211.

[46] Cahoy JD, Emery B, Kaushal A, Foo LC, Zamanian JL, Christopherson KS, et al. (2008). A transcriptome database for astrocytes, neurons, and oligodendrocytes: a new resource for understanding brain development and function. J Neurosci, 28:264-278.